

Alloy Formation by Arc Deposition of AISI 308 Reinforced with Titanium-Graphite Powder and Wear Properties of the Alloy Surface Coat

T. Vigraman*, N. Nanda Gopal, M. Muthu Kumaran, M. Raghul, G. Raj Kumar

Department of Mechanical Engineering, National Engineering College, Kovilpatti – 628503, Tamil Nadu, India;
tvr@nec.edu.in, nandagopal344@gmail.com, muthukumarankar@gmail.com,
ragul1809@gmail.com, mechanicalrajkumaru@gmail.com

Abstract

Objectives: To prepare a wear resistant surface and to induce compressive stress on the AISI 304L steel by depositing titanium-graphite powder in a matrix of AISI 308 steel. **Methods/Statistical Analysis:** The coating is deposited using manual metal arc welding (MMAW) process with a current value set at 125 amp and 70 volt. The alloy element titanium is added upto 1, 1.5 and 2% and carbon content is maintained at 0.3%. The coated samples are heated with oxy-acetylene flame and impact force is applied on the coated surface during heat treatment, to ensure penetration of the hard particles. Further, compressive stress is induced on the surface because of the applied impact force. The coated surface is finished in a surface grinding machine to obtain a flat smooth surface. Hardness assessment is carried out on the coated surface using Rockwell hardness measuring machine. **Findings:** A maximum hardness value of Rc55 is obtained for the sample containing 1% titanium and 0.3% carbon. Pin on disc experiment is conducted on the samples to estimate the wear rate. The Scanning Electron Microscopy (SEM) examination revealed the presence of various carbides in the alloy. Energy Dispersive X-ray Analysis (EDAX) is performed to find out composition of the coating. **Application/Improvements:** The wear resistant coating could be used in corrosive environment. Shafts can be arc deposited and compressive stress can be induced on the surface using a blunt tool fitted with the tool post of a lathe. This alloy can be used as a wear resistant coat and as a bearing material.

Keywords: Austenite Grains and Oxides, Carbides, Intermetallic Compounds, Micrograph

1. Introduction

The austenitic stainless steel AISI 304L is a weldable grade stainless steel possessing good mechanical and corrosion resistant properties. The high temperature properties coupled with oxidation resistant properties makes these grades of stainless steels as suitable tubular material for thermal power plant applications¹. Further, AISI 304L has good ductility and formability. But AISI

304L possess inferior wear resistant properties. By providing coatings on the surface, the erosion assisted wear resistant properties of AISI 304L are enhanced². Studied the wear behavior of SUS 304 steel disc by varying load and sliding speed against Al_2O_3 ceramic ball in a pin on disc testing machine. Further, the study was carried out for understanding the effect of strain hardening and wear properties on the tool life during forming. Wear resistance is enhanced by providing heat-treatments such as

*Author for correspondence

quench hardening and surface hardening. Further, various surface modification techniques are adopted on the substrate material to obtain hard wear resistant surface. Among them plasma spraying, oxy-fuel spraying, laser beam surface modification and arc deposition techniques are very widely used.

The manual metal arc welding (MMAW) process is less expensive compared to other processes such as metal inert gas welding (MIG) and plasma welding. Because of high heat input the deposition rate is high in both the processes. The equipment and consumable cost is low in MMAW. In³ performed infiltration of AISI 316 into the TiC performs having two different grain sizes in a vacuum furnace. The maximum hardness value was obtained in the fine grained TiC. Further, the wear rate was minimum in the fine grain billets. The surface of the wear test specimens revealed extrusion of the binder AISI 316 and TiC fragmentation during sliding wear process. ⁴Prepared Fe₃Al coating reinforced with TiB₂ on alumina substrate using high velocity oxy fuel spraying technique. A titanium carbide-metal composite was prepared by adopting powder metallurgy technique⁵.

In the present study a modified manual metal arc welding process is used to prepare the alloy and to deposit on the surface of AISI 304L. The titanium and graphite powder mixture is supplied at the arc region, so that complete fusion of the powder with the electrode AISI 308 takes place. This alloy can be used as a wear resistant coat and as a bearing material.

2. Experimental Work

The base metal AISI 304L stainless steel in the form of flat plate 60 mm wide and 3 mm thick is cut to cuboids of 60×50×3 mm in size. The composition of the base metal and the filler material AISI 308 coated electrode is given in Table 1. The composition of the filler metal is varied by adding titanium and carbon powder at 1, 1.5 and 2%Ti and 0.3% C. The experimental order is sample 1, sample 2 and sample 3 having 1, 1.5 and 2% Ti, respectively. The filler metal is deposited with electric arc welding process using AC power source. The arrow marks shown in Figure 1 represents the chemical reaction between the molten metal and powder mixture. The welding parameters are set at 125 Amp and 70 volt. The electric arc deposited samples are given post heat-treatment using oxy-acetylene flame to obtain homogeneous deposition on the substrate. A model of the electric arc deposited specimen is shown in Figure 2.

The hardness assessment is carried out in a Rockwell hardness testing machine using 'C' scale. A test load of 150 Kg is applied while assessing hardness values. The metallography and hardness specimens are cut to cuboids of size 15×10×5 mm. The metallography specimens are prepared by polishing with silicon carbide abrasive sheets having grit size 180, 220, 320, 400, 600, 800, 1000 and 1200. These samples are further finished in a disc polishing machine using 0.1 and 0.05 micron alumina slurry. The polished specimens are etched with a mixture con-

Table 1. The chemical composition of the base metal and filler metal

Element Wt %	C	Cr	Mn	Ni	P	S	Si
AISI 304L	0.03	18	2	8	0.05	0.03	1
AISI 308	0.08	20	2	11	0.05	0.03	1

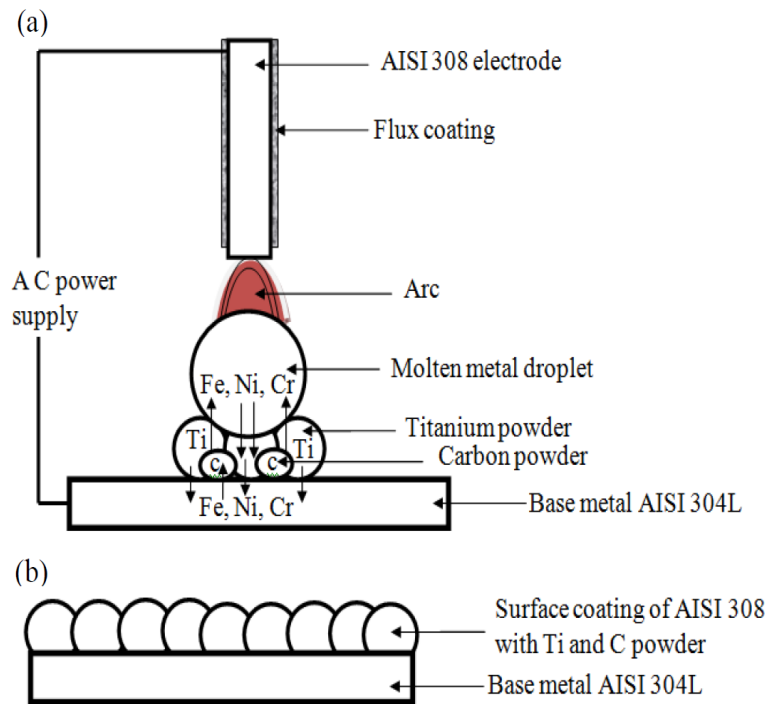


Figure 1. (a). A schematic diagram showing the electric arc deposition and (b) model of the arc deposited sample.

taining 5ml HCl+10 ml HNO_3 +2%Picral+0.05g NH_3HF_3 . The wear test is conducted based on the ASTM standard G-99⁶. The wear test specimens of 8×8×3 mm square section are prepared and a cylindrical shank portion is prepared by welding a mild steel pin with the cuboid wear test specimen. The sliding speed is maintained at 2 m/s for all the experiments.

3. Results and Discussions

3.1 Optical Microscopy

The micrograph shown in Figure 2 reveals the presence of titanium carbide as greenish round particles. These particles are dispersed throughout the matrix. At few places these particles are finer and a few places they are coarse. Along with TiC at the grain boundary and closer to the grain boundary brown particles are

seen. These particles are chromium carbides (CrC). The microstructure consists of coarse grains and few fine grains. At few places small grains are noted, these grains are formed because of recrystallization and grain refinement during solidification. At the grain boundary triple points segregation of carbides are noted. The grain boundaries and triple points are the high energy regions where chemical reaction takes place because of migration of chromium atoms. Few grain boundaries are visible and at the other regions they are suppressed because of difference in etch rate.

Figure 2 fines green and brown colour particles are seen throughout the matrix. These particles are TiC and CrC. The titanium carbides are grayish in colour and irregular in shape⁷. Intermetallic compounds such as Ti Fe₂ and Ti Ni₂ are identified as Laves phase which precipitates intragranular and exists as globular particles⁷. At few places very fine grains are noted and these grains are

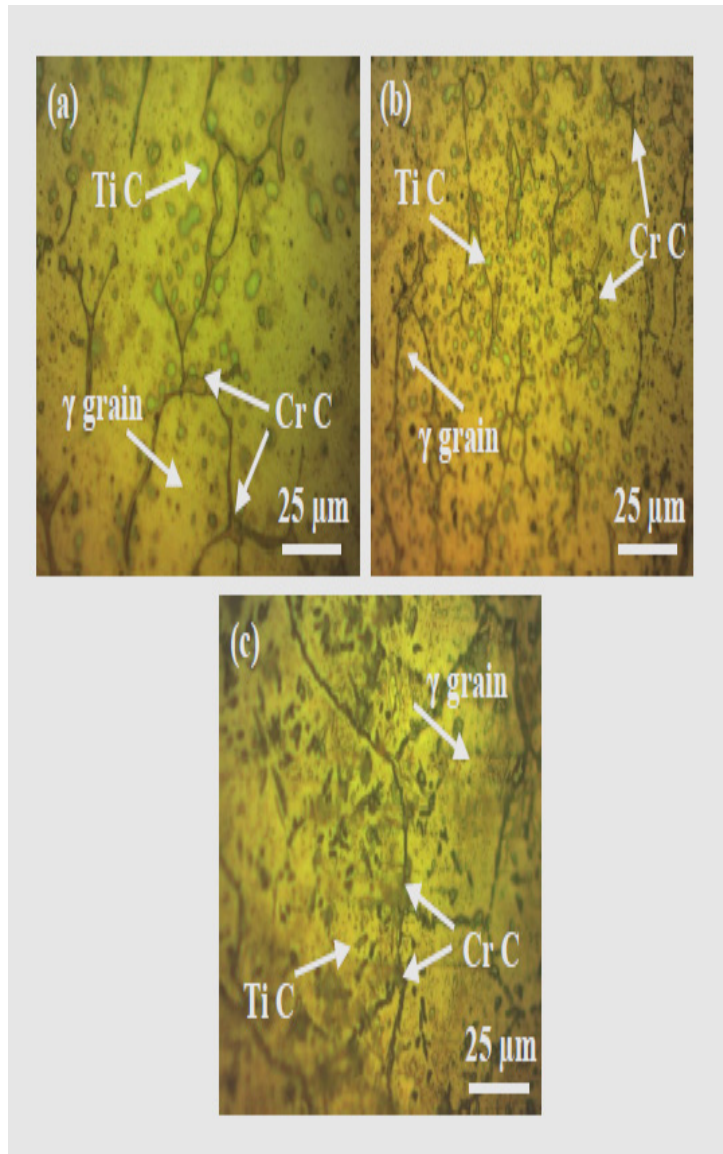


Figure 2. Optical micrographs of the samples coated with (a) 1%Ti and 0.3%C powder, (b) 1.5% Ti and 0.3%C (b) powder and (c) 2% Ti and 0.3%C powder.

formed because of recrystallization and grain refinement during solidification. In comparison with the Figure 2, the microstructure presented in Figure 2 has more amounts of carbides. The rise in titanium carbide content is attributed to increase in titanium upto 0.3% Ti addition in the AISI308 steel. At few regions very fine dark particles are

seen and these particles are identified as titanium oxide (TiO_2).

The very small grains in green shade are rich with titanium and other alloying elements. These grains are formed because of recrystallization and grain refinement during solidification. The austenite grains are very small

compared to the grains observed in Figure 2. At the bottom side of the micrograph a dark line which is identified as a grain boundary is visible. On either side of the grain boundary epitaxial growth is noted at few places across the length of the line. This indicates dendrite formation in the solidified metal further, the discontinuous dendrites are noted because inoculants such as titanium and carbon in the alloy.

The micrograph shown in Figure 2 corresponds to the sample 3. The austenite grains are coarse and only few grains are seen in this micrograph. The carbide segregation along the grain boundaries are less, therefore, the grain boundary is thin. At few places spherical carbides are seen, adjacent to the grain boundary brown shaded regions are seen which are rich with TiC and CrC type of carbides⁷. The grain matrix has several such brown shaded regions. In this micrograph at several places the presence of needle like phase is noted. This phase is a mixture of TiC and identified as β -titanium rich with elements such as Fe, Cr, Ni and Si. The reason for presence of this phase is increase in Ti addition in this alloy which is upto 0.5%.

3.2 SEM Microscopy

The SEM micrograph shown in Figure 3 reveals the presence of titanium carbide which is in the form of dark particles and these thick particles are dispersed throughout the matrix. The fine white particles are identified as CrC. These particles are distributed evenly throughout the matrix. The formation and morphology of chromium carbide is as in the cited work⁸. Further, at few places white round particle are seen and these particles are TiO_2 . The matrix is grey in colour which is surrounded by dark particles. These particles are thick and are precipitated along the grain boundaries. The micrograph shown in Figure 3 is taken at higher magnification corresponds to the sample 1. A dark wedge like profile is seen in the micrograph which is rich with CrC and TiC carbides. At the top and bottom ends of the wedge white particles are seen and these particles are TiC and TiO_2 . The carbon solubility in α and β -Ti is in the range of 0-0.4% and 0-0.2%, respectively which is presented by⁹ in the phase diagram drawn between carbon and titanium. Titanium has greater affinity to carbon, therefore, TiC (10-19.3%C)

and Ti_2C (10-12.4%C) type of carbides are formed. A dark grey region is seen on the top side of the micrograph which is rich with β -Ti. Further, this region is rich with β -stabilizing elements such as Fe, Cr, Ni, Si and Mn.⁹ Revealed (in the phase diagram drawn between Ni-Ti and Fe-Ti) the formation of β -Ti because of presence of 0-12%Ni and 0-24.7% Fe. Large austenite grains and fine white TiC particles are seen in the matrix.

The SEM micrograph shown in Figure 3 reveals fine white particles which are identified as TiC. These particles are distributed homogeneously in the micrograph. At the centre of the micrograph a dark grey region rich with Cr_6C and $Cr_{23}C_6$ is seen.¹⁰ Noted cast dendritic structure formation during solidification of the molten TiC and AISI 304. A similar structure is observed in the SEM micrograph shown in Figure 3. Adjacent to this on the left side of the micrograph a white elongated region is noted which is rich with TiC.¹¹ Discussed sufficient Ti content is essential so that all the carbon present in the alloy is transformed to TiC, otherwise $M_{23}C_6$ carbides could be formed. Presence of chromium carbides and titanium carbides corroborates the observations made¹¹. The grey region is more in volume than white region in this micrograph. This region is rich with β -stabilizing elements such as Fe, Cr, Ni, Si and Mn. Figure 3 a white curvy region is noted and this region is identified as austenite grain. At the bottom side a dark region is seen which is rich with intermetallic compounds such as Fe_2Ti , and FeCrTi type σ -phase. The SEM micrograph taken at higher magnification reveals the presence of a curved region rich with carbides in the austenite grain. This region is broken into small parts and the edges are whitish in colour. The white border lining is rich with TiC and TiO_2 . The phase diagram between Titanium -Oxygen by¹² revealed the solubility of oxygen in β -Ti and α -Ti as 0-0.3% and 0-13.5%, respectively. A crack like grain boundary is visible because of more etching time given to the sample. At the grain boundary triple point a dark region is visible which is rich with CrC and TiC. Further, several fragmented dark grey regions are observed. Furthermore, these region are rich with β -stabilizing elements such as Fe, Cr, Ni, Si and Mn. Few grayish white region are noted which are large γ -grains.

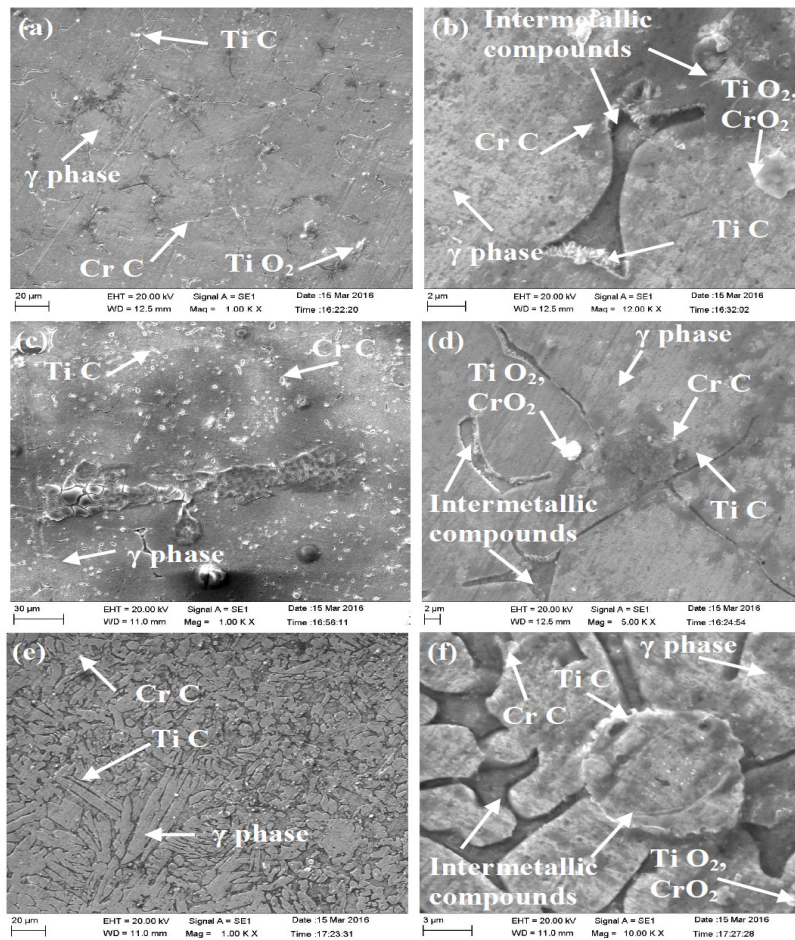


Figure 3. SEM images of the samples coated with (a)-(b) 1% Ti and 0.3% C powder, (c)-(d) 1.5% Ti and 0.3% C powder and (e)-(f) 2% Ti and 0.3% C powder.

Figure 3 dark needle like structure adjacent to the austenite grains are seen. These needles are identified as β -phase. This phase is rich with β -stabilizing elements such as Fe, Cr, Ni, Si and Mn. Among the SEM micrographs shown in Figure 3 have very fine austenite grains. At few places dark round and elongated particles are seen and these particles are CrC and TiC. The amount of carbides, intermetallic compounds and oxides such as TiC, CrC, Fe_2Ti , σ -phase are more because of more percentage of Ti addition in the AISI 308 alloy.

The presence of these phases is confirmed¹³. The SEM micrograph shown in Figure 3 is taken at higher magnification. Many fine needles like dark elongated regions are seen. These needles are rich with β -stabilizing elements such as Fe, Cr, Ni, Si and Mn. Further, more amounts of TiC and CrC carbides are present in this region. The grey regions in the micrograph are identified as γ -grains. A large circle is visible at the centre which is identified as TiC. Further, at one or two places dark islands are visible and these regions are rich with various carbides.

3.3 Energy Dispersive X-Ray Analysis

The energy dispersive X-ray analysis (EDAX) performed on the surface revealed the presence of titanium and carbon on the coated material along with elements present in the AISI 308 steel. The point scan performed on the surface indicated the presence of the elements such as Fe, Ni, Cr, Si, Mn, Ti, and C. Carbides such as TiC and CrC are formed when carbon is present along with Ti and Cr. Further, Ti readily forms intermetallic compounds Fe_2Ti , Ni_2Ti and $FeCrTi$ in liquid state with Fe and Ni. The point scan details of the EDAX report is given in Table 2. A maximum of 2.26% Ti is present at a point on the coated material.

Therefore, presence of compounds such as Fe_2Ti , $FeCrTi$, TiC and CrC type of carbides are inevitable. The EDAX report presented in the work¹³ confirmed the presence of the above mentioned phase. Further, the EDAX report shown in Figure 4 reveals the presence of oxygen in the coating material. During arc welding process infiltration of interstitial element oxygen cannot be prevented.

Further, CrO_2 is present on the surface of the base metal AISI 304 L stainless steel which gets dissolved during arc melting of the filler metal. Therefore, presence of oxides such as TiO_2 and CrO_2 is confirmed with EDAX report.

In the EDAX report shown in Figure 4 oxygen is not present. This indicates effective shielding of the molten metal from interstitial elements such as oxygen, hydrogen, nitrogen and other gases. This indicates the base metal surface is effectively cleaned to remove CrO_2 with buffing process before arc deposition. The point scan performed on the surface of sample 2 indicated the presence of the elements such as Fe, Ni, Cr, Si, Mn, Ti, and C. Titanium has greater affinity to form carbide than chromium. Therefore, TiC and CrC type of carbides are formed when carbon is present along with Ti and Cr. Also, Ti readily forms intermetallic compounds in liquid state with Fe and Ni. A maximum of 1.44% Ti is present at a point on the coated material. The decrease in Ti content is attributed to dilution of the titanium from the coated metal and segregation of the element because of the tech-

Table 2. The EDAX report taken on sample 1 and 2 at two points

Element	Sample 1		Sample 2	
	Point 1	Point 2	Point 1	Point 2
	Wt %	Wt %	Wt %	Wt %
Iron	63.36	63.99	66.93	67.01
Chromium	16.91	17.07	16.74	17.15
Nickel	7.29	7.37	7.47	7.89
Carbon	5.7	5.81	5.65	4.57
Titanium	2.21	2.23	1.16	1.32
Oxygen	1.78	0.00	0.00	0.00
Manganese	1.58	1.6	1.49	1.59
Silicon	0.72	0.73	0.7	0.83

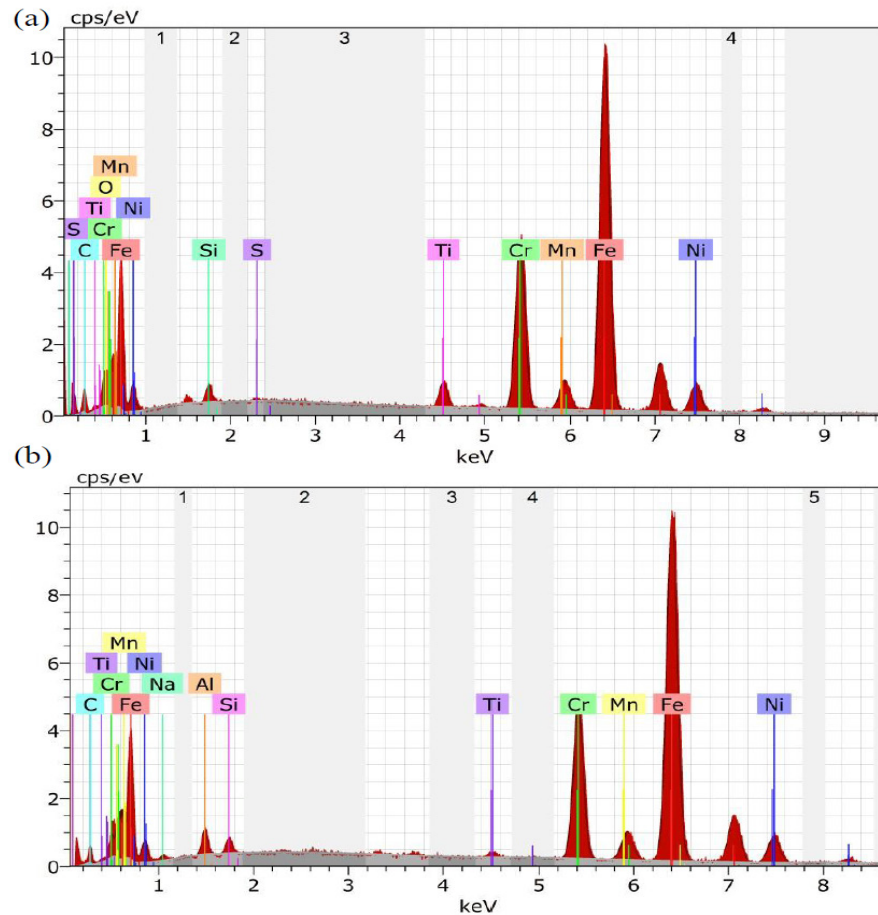


Figure 4. (a) The EDAX report for the sample 1 and (b) for the sample 2.

nique adopted. In ¹⁴Estimated the amount of carbon and oxygen in the composite by performing EDAX on the surface of the wear tests samples. The oxygen and carbon content is measured and presented in accordance with the work¹⁴. Therefore, presence of compounds such as TiC, CrC, Fe₂Ti, Ni₂Ti and FeCrTi are inevitable. Further, the EDAX report for the sample 2 taken at two points is given in Table 2 which reveals the absence of oxygen in the coating material. Therefore, presence of oxides such as TiO₂ and CrO₂ is not observed in the EDAX report.

This indicates effective shielding of the molten metal from interstitial elements such as oxygen, hydrogen, nitrogen and other gases.

3.4 Rockwell Hardness Values

The hardness values were measured across the length of the coated material. The average hardness value of the base metal AISI 304 L is only Rc15 in Rockwell ‘C’ scale. After depositing the AISI 308-Ti-C coating on the surface

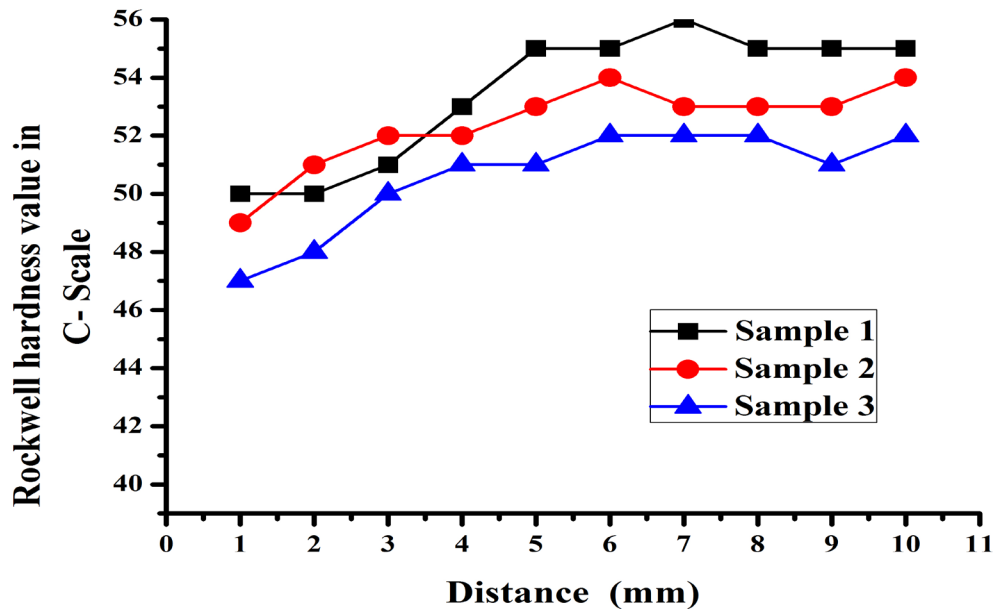


Figure 5. A graphical plot of Rockwell hardness values on the surface of the coated samples.

the surface Rockwell hardness values were on the rise. A graphical plot between the distance across the length of the coated sample and the Rockwell hardness values in C scale are shown in Figure 5. A maximum of Rc 55 was recorded on the surface at a point. At the recrystallized zone the average hardness value was 55 on hard surface. In ¹⁴Observed the hardness of the metal matrix composite AISI 304 and TiC was on the rise with respect to rise in TiC content in the composite. In the present study the hardness values are on the rise for the alloy having more Ti addition which indicates presence of more amounts of carbides such as TiC, Cr₆C and Cr₂₃C₆.

In the weld metal hardness values were on the rise because of diffusion of interstitial elements such as oxygen, hydrogen and nitrogen into the weld metal. Further, elements like titanium and carbon diffuses from the base metals to the weld metal, thus increased hardness values were realized. The rise in hardness value is attributed to the formation of intermetallic compounds, carbides and oxides on the coating. At the recrystallized zone fine

grains were formed, these small grains increase hardness value up to 52-55. ¹⁵Performed surface modification on steel for raising the wear resistance properties with TiC and realized a maximum hardness of Rc 70. ¹⁶Observed during vapour deposition technique Ti and C diffused into tool steel in austenitic state at a temperature range of 900-1050 °C to form TiC. In the current work a maximum hardness of Rc55 is realized because of in homogeneity in the distribution of Ti and lack of complete transformation of TiC in the deposited metal. Further, Ti addition is only 1-2% because of this α and β -Ti might have formed instead of hard intermetallic compound formation.

3.5 Wear Resistance

The graphical plot shown in Figure 6 is drawn between the load and the wear loss. As the load on the pin is raised the wear loss increases and reaches a maximum value for the sample 1. The wear loss estimated for all the three samples reinforced with Titanium and carbon is very

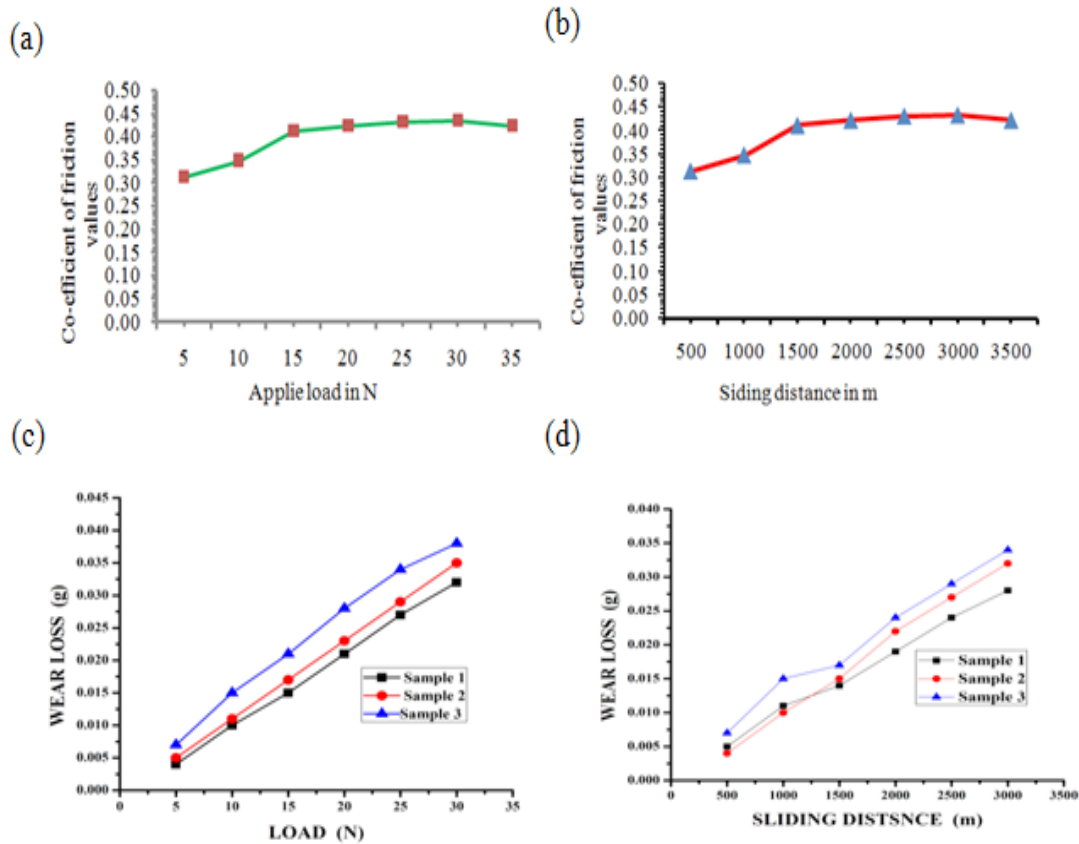


Figure 6. A graphical plot between (a) applied load vs. co-efficient of friction, (b) sliding distance vs. co-efficient of friction, (c) load vs. wear loss and (d) sliding distance vs. wear loss.

less when it is compared with the test results of AISI 304 stainless steel. In this case the wear is less because of the formation of intermetallic compounds and carbides such as TiC, CrC, Fe₂Ti, Ni₂Ti and FeCrTi in a softer austenite matrix. The wear test specimens were observed through optical microscope for wear pattern. The maximum wear rate of 0.034 g/min is obtained for the sample having 1% Ti and 0.3% C and a minimum wear rate of 0.024 g/min is recorded for the sample having 2% Ti and 0.3% C. The wear test specimens were observed through optical microscope for wear pattern. The micrographs shown in Figure 7 for the sample 1 reveals scratch marks and wears at localized regions. This indicates the softer phase is

worn out and the hard phases present in the alloy are left as it is on the surface. The broken and torn away regions seen in the micrograph reveals the area where such hard phases are present more. A minimum wear loss is noted for the sample 1 because of more amounts of titanium and carbon present in the alloy. Wear loss is indirectly proportionate to the alloy content and amount of intermetallic compounds and carbides present in the alloy. The average co-efficient of friction value obtained from the pin on disc experiment is 0.398.

A graphical plot shown in Figure 6 is drawn between the sliding distance and wear loss. As the sliding distance of the pin is increased the wear loss increases and reaches

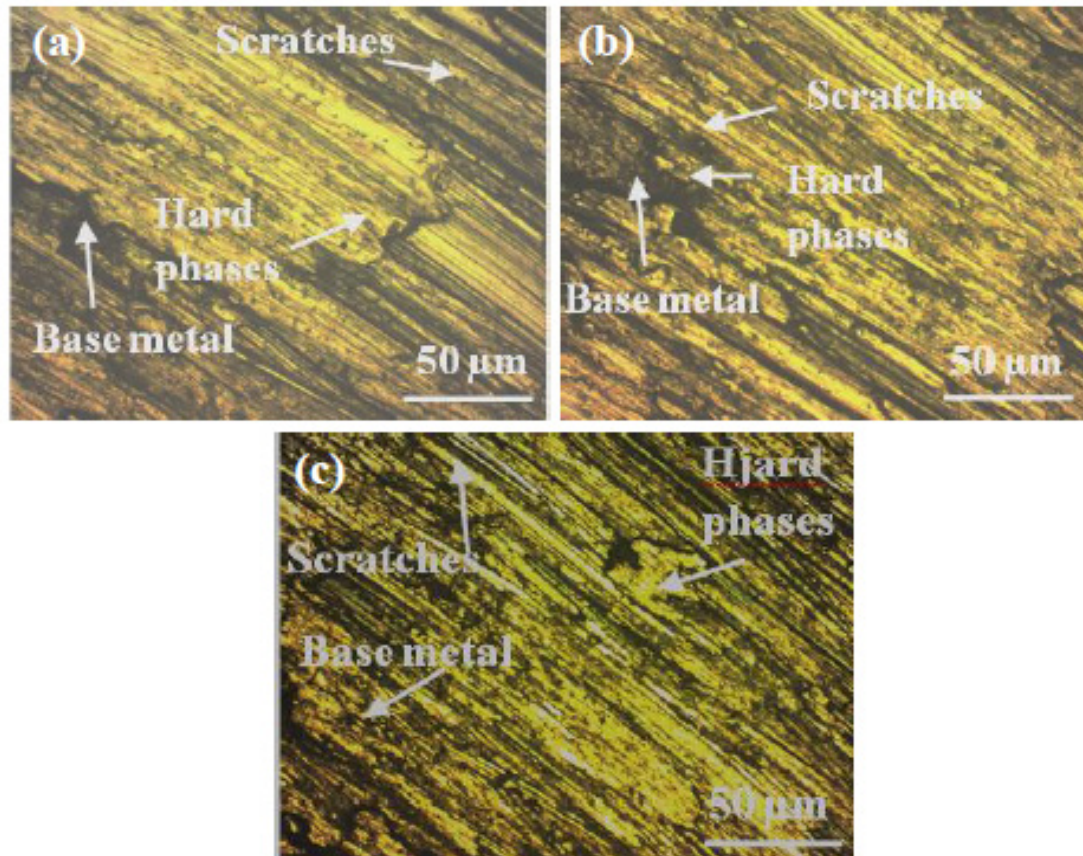


Figure 7. The optical micrographs shows wear pattern of a) the sample 1, b) sample 2 and c) sample 3.

a maximum value for the sample 1. The wear loss estimated for all the three samples reinforced with Titanium and carbon is very less when it is compared with the test results of AISI 304 stainless steel. In this case the wear is less because of the formation of intermetallic compounds and carbides such as TiC, CrC, Fe₂Ti, and FeCrTi in a softer austenite matrix. A minimum wear loss is noted for the sample 3 because of more amounts of titanium and carbon present in the alloy. Wear loss is indirectly proportionate to the alloy content and amount of intermetallic compounds and carbides present in the alloy.

The wear test specimens were observed through optical microscope for wear pattern. The micrographs shown in Figure 7 reveals very fine scratches marks and wear at localized regions. This indicates the softer phase is worn out and the hard phases present in the alloy are left as it is on the surface. The broken and torn away regions seen in the micrograph reveals the area where such hard phases are present more. The wear track observations are in accordance with the observations made¹⁷. The wear pattern formed on the surface of the specimen 2 is shown in Figure 7.

The micrographs showed in Figure 7 reveals very fine scratches marks in comparison with the Figure 7 and minimum wear at localized regions. This indicates wearing of the softer phase in small amounts because more amounts of hard phases are present in the alloy than in the sample 1. The micrographs showed in Figure 7 reveals very fine scratches marks in comparison with the Figure 7 and minimum wear at localized regions. This micrograph corresponds to the sample 3. This indicates wearing of the softer phase in small amounts because more amounts of hard phases are present in the alloy than in the sample 2. In the micrograph a small hole is seen which is formed because of removal of intermetallic compounds from the softer matrix austenite phase.

The broken and torn away regions seen in the micrograph reveals the area where such hard phases are present. In ¹⁸Revealed during wear testing relative motion existed between disc and pin which ensured adhesive bonding between contacting surfaces, because of this fracturing of the softer phases resulted. Tearing of the softer phase is observed at the contact points where hardness is less and adhesive bonding existed. Wherever abrasive wear is observed the wear track is in the form of scratch marks. As the hardness values are more the scratches are light and at the regions where hardness is less deep scratches are observed.

4. Conclusion

- The surface modification on AISI 304 L base metals with AISI 308 and Ti-C is successfully carried out with arc deposition technique. The transformed alloy was having homogeneous phase distribution of secondary phases in it.
- The microscopic examination of the samples revealed the presence of carbides, oxides and intermetallic compounds in the coated material.
- Presence of intermetallic compounds such as Fe₂Ti, FeCrTi, and carbides namely TiC and CrC are noted. Further, presence of oxides such as CrO₂ and TiO₂ were noted.

- A maximum hardness of Rc 55 is obtained for the sample deposited at 125 Amp and 40 V because of formation of hard intermetallic compounds and carbides.
- The wear properties are enhanced with the addition of Ti-C powder because of formation of hard carbides and intermetallic compounds in the alloy.

5. References

1. Vigraman T, Ravindran D, Narayanasamy R. Diffusion bonding of AISI 304L steel to low-carbon steel with AISI 304L steel interlayer. *Materials and Design*. 2012 Feb; 34:594-602. CrossRef.
2. Hua M, Wei X, Li J. Friction and wear behavior of SUS 304 austenitic stainless steel against Al₂O₃ ceramic ball under relative high load. *Wear*. 2008; 265(5-6):799-810. CrossRef.
3. Chukwuma C Onuoha, Georges J Kipouros, Zoheir N Farhat, Kevin P Plucknett. The effects of TiC grain size and steel binder content on the reciprocating wear behaviour of TiC-316L stainless steel cermets. *Wear*. 2016; 350:116-29.
4. Amiriyani M, Blais C, Savoie S, Schulz R, Gariépy M, Alamdari H. Tribo-Mechanical Properties of HVOF Deposited Fe₃Al Coatings Reinforced with TiB₂ Particles for Wear-Resistant Applications. *Materials*. 2016; 9(2):117. CrossRef.
5. Hussainova I. Effect of microstructure on the erosive wear of titanium carbide-based cermets. *Wear*. 2003; 255(1-6):121-8. CrossRef.
6. Standard Test Method for Wear Testing with a Pin-on-Disk Apparatus. *Annual Book of ASTM Standards*. Designation G 99 - 95a. 2000; p. 1-6.
7. Voort GFV, Lucas MG, Manilova EP. *Metallography and Microstructures of Stainless Steels and Maraging Steel*. ASM Handbook ASM International. 2004; 9: 670-700
8. Vigraman T, Ravindran D, Narayanasamy R. Microstructure and mechanical property evaluation of diffusion-bonded joints made between SAE 2205 steel and AISI 1035 steel. *Materials and Design*. 2012; 35:156-69. CrossRef.
9. Murray JL. *Alloy Phase Diagrams*. ASM Handbook ASM International. 1991; 3:539-1259.
10. Mahmoud RIE. Microstructure, Wear and Corrosion Characteristics of 304 Stainless Steel Laser Cladded With Titanium Carbide. *International Journal of*

- Engineering Research and Technology (IJERT). 2015 Aug; 4(8):422-7.
11. Sourmail T. Precipitation in creep resistant austenitic stainless steels. *Material Science and Technology*. 2001 Jan; 17:1-14. CrossRef.
 12. ASM Handbook. Alloy Phase Diagrams ASM International. 2016; p. 1-9.
 13. Vigraman T, Ravindran D, Narayanasamy R. Effect of phase transformation and intermetallic compounds on the microstructure and tensile strength properties of diffusion-bonded joints between Ti-6Al-4V and AISI 304L *Materials and Design*. 2012 Apr; 36:714-27.
 14. Chukwuma C Onuoha, Georges J Kipouros, Zoheir N Farhat, Kevin P Plucknett. The reciprocating wear behavior of TiC-304L stainless steel composites prepared by meltinfiltration. *Wear*. 2013; 303:321-33. CrossRef.
 15. Budinski KG. New Jersey, Prentice Hall: *Surface Engineering for Wear Resistance*. 1988.
 16. Michael J Schneider and Madhu S Chatterjee. Introduction to Surface Hardening of Steels Heat Treating. ASM Handbook ASM International. 1991; 4:259-67.
 17. Sun Y. Sliding wear behavior of surface mechanical attrition treated AISI 304 stainless steel. *Tribology International*. 2013; 57: 67-75. CrossRef.
 18. Hsu CH, Huang KH, Lin YH. Microstructure and wear performance of arc-deposited Ti-N-O coatings on AISI 304 stainless steel. *Wear*. 2013; 306:97-102. CrossRef.